

Assessment of EFM as a new nondestructive technique for monitoring the corrosion inhibition of low chromium alloy steel in 0.5 M HCl by tyrosine

Mohammed A. Amin · Sayed S. Abd El Rehim ·
M. M. El-Naggar · Hesham T. M. Abdel-Fatah

Received: 18 June 2009 / Accepted: 27 August 2009 / Published online: 18 September 2009
© Springer Science+Business Media, LLC 2009

Abstract Electrochemical frequency modulation (EFM), a nondestructive corrosion measurement technique that can directly give values of corrosion current without prior knowledge of Tafel constants, is applied here to investigate the inhibition performance of tyrosine (Tyr) toward corrosion of low chromium alloy steel in 0.50 M HCl. Measurements were conducted under various experimental conditions in the range of temperature (20–60 °C). Results obtained from EFM were compared with other traditional corrosion monitoring techniques, namely Tafel extrapolation, impedance, and weight loss. Polarization measurements showed that Tyr acted as a mixed-type inhibitor with cathodic predominance. The inhibition process was attributed to the formation of an adsorbed film on the metal surface that protected the metal against corrosive agents. Energy dispersive X-ray spectroscopy and scanning electron microscopy examinations of the electrode surface confirmed the existence of such an adsorbed film. The inhibition efficiency increased with increase in Tyr concentration, while it decreased with solution temperature. The adsorptive behavior of Tyr on the electrode surface followed Temkin-type isotherm. Thermodynamic functions for the adsorption process were determined. The data obtained from the different methods were in good agreements, which

indicated that the EFM technique was valid for monitoring the corrosion inhibition under the studied conditions.

Introduction

The fossil fuel fired boilers experience corrosion problems in both waterside and fireside tubing system such components as steam generators, waterwalls surrounding the furnace, superheater, and reheater [1–3]. These components are often made of low carbon and low alloy steels. The corrosion inhibition of low chromium alloy steel SA213-T22 becomes of such interest because it is widely used for manufacturing the steam generating sections of boilers [4, 5].

The internal surfaces of a boiler in contact with water and steam must be kept clean and free of deposits to assure efficient heat transfer in the generation of steam [6]. The water used for steam raising in any boiler installation often contains gaseous impurities and dissolved solids. The consequences of the buildup of scale and the accumulation of deposits are the possible causes of the degradation of the tubes and the increased possibility of overheating and failure [7–10].

Such scale is normally removed by acid cleaning [11]. Several solvents will effectively remove waterside deposits. Mostly, hydrochloric and sulfuric acids are employed for such purpose [12]. Hydrochloric acid is widely used for the removal of rust and scale in several industrial processes such as industrial acid cleaning, oil well acidizing, acid pickling and removal of oxide from metallic parts before applying coating [13].

Inhibitors are generally used in these processes to control the metal dissolution. Most of the well-known acid inhibitors are organic compounds containing nitrogen, sulfur, and oxygen atoms. This phenomenon is influenced by the nature and surface charge of metal, by the type of

M. A. Amin (✉) · S. S. Abd El Rehim
Chemistry Department, Faculty of Science, Ain Shams
University, Abbassia, Cairo, Egypt
e-mail: maaismail@yahoo.com

M. M. El-Naggar
Chemistry Department, Faculty of Science,
Benha University, Benha, Egypt

H. T. M. Abdel-Fatah
Central Chemical Laboratories, Egyptian Electricity Holding
Company, Sabtia, Cairo, Egypt

aggressive electrolyte, and by the chemical structure of inhibitor [14–19]. The corrosion inhibitors and their use in specific applications such as the acid cleaning of steam generators are shortly reviewed [20].

The strict environmental regulations and the increasing of ecological awareness have resulted in the use of substitute nontoxic compounds, acceptable from the environmental point of view “green inhibitors” [21, 22].

Unfortunately, many common corrosion inhibitors are health hazards. The inhibition effect of amino acids on the corrosion of iron, steel and stainless steel were reported [23–27]. Amino acids are environmentally friendly compounds. In addition, amino acids are from a class of organic compounds, relatively easy to produce with high purity at low cost and completely soluble in aqueous media. These properties would justify their use as corrosion inhibitors [22, 28]. Glycine was used as a safe-inhibitor for the acid corrosion of the low chromium alloy steel [29].

Electrochemical frequency modulation, EFM, is used as a new technique for corrosion rate measurements [30–32]. In EFM technique, two AC voltage waveforms are summed and applied to the LCS electrode. The frequencies of the two sinusoidal waveforms must share no common factors. Normally, 2 and 5 Hz are suitable frequencies for EFM. While simple in concept, EFM yields an impressive amount of information on the corrosion process including corrosion rate, Tafel constants, and causality factors. The corrosion rate is calculated from the corrosion current density that is measured by EFM [31].

It is worth emphasizing that the Tafel constants are not needed to measure the corrosion current density. For this reason, EFM enjoys a significant practical advantage compared to polarization techniques. EFM provides an independent measure of the anodic and cathodic Tafel constants. The causality factors are used to validate the data. The causality factors are similar to an internal check of the consistency of the measurement process. There are two causality factors (2) and (3); if the calculated causality factors are higher than 2 and 3, respectively, the quality of the measured data is not valid. Additionally, EFM may be less susceptible to errors in applied potential from IR effects than polarization measurements.

Bogaerts and co-workers [31, 32] proposed EFM as a novel technique for online corrosion monitoring. In this technique, current responses due to a potential perturbation by one or more sine waves are measured at more frequencies than the frequency of the applied signal, for example at zero, harmonic and intermodulation frequencies. EFM can be used successfully for corrosion rate measurements under various corrosion conditions, such as iron in acidic environment without and with inhibitors and mild steel in a neutral environment.

However, Kus and Mansfeld [33] evaluated the EFM technique for several corrosion systems including active and passive systems and found that EFM measurements can be applied successfully only for a limited number of corrosion systems with fairly high corrosion rates and the technique should be used only with great caution for corrosion monitoring. Recently, Han and Song [34] set up a system for EFM measurement for the early corrosion rate of mild steel in sea water system.

In this study, and in a continuation of our previous study [29], the inhibition performance of tyrosine (Tyr), a nontoxic compound, was tested toward the low alloy steel (T22) corrosion in 0.5 M HCl solution. For this purpose, various corrosion monitoring techniques, namely Tafel extrapolation, impedance and weight loss were used. It was also the purpose of this study to evaluate EFM as a new nondestructive technique against the traditional corrosion monitoring methods.

Experimental

The working electrodes employed in this study were made of low alloy steel (ASTM A213 grade T22), this type of alloy are widely used as a super-heater pipes at steam power plants. The compositions of the low alloy steel were determined using energy dispersive X-ray spectroscopy (EDX) and presented elsewhere [29]. All solutions were freshly prepared from analytical grade chemical reagents using doubly distilled water. Each run was carried out in stagnant aerated solutions at the required temperature.

The weight loss experiments were performed with low alloy steel strips of approximate dimensions ($2.0 \times 2.0 \times 0.6 \text{ cm}^3$). All coupons were polished successively with fine grade emery papers, degreased with acetone, washed with doubly distilled water, and finally dried. The weight loss, expressed in mg cm^{-2} , was determined by weighing the cleaned samples before and after immersion in the test solution. The experiments were carried out in 0.5 M HCl solutions without and with various concentrations (1.0–50 mM) of Tyr at different immersion times and temperatures.

For electrochemical measurements, the investigated materials were cut as cylindrical rods, welded with Cu-wire for electrical connection and mounted into glass tubes of appropriate diameter using Araldite to offer an active flat disc-shaped surface of (1.0 cm^2) geometric area, to contact the test solution. Prior to each experiment, the surface pretreatment of the working electrode mentioned in weight loss measurements was performed. The experiments were performed in a 150 cm^3 volume cell, using Pt foil (1.0 cm^2) and a SCE as auxiliary and reference electrodes, respectively. The SCE was connected via a Luggin capillary, the tip of which was very close to the surface of the working electrode

to minimize the IR drop. Experiments were carried out at the required temperature (± 2.0) using a temperature control water bath. The cell was open to air and the measurement was conducted at room temperature. All potential values were reported in volt (SCE).

Polarization measurements were carried out starting from a cathodic potential of -0.65 V to an anodic potential of 0.0 V at scan rate 0.50 mV s^{-1} . The linear Tafel segments of the cathodic curves and the calculated anodic Tafel lines (see more details in our previous study [29]) were extrapolated to corrosion potential to obtain the corrosion current densities (j_{corr}).

Impedance measurements were carried out using AC signals of amplitude 5 mV peak to peak at the open circuit potential in the frequency range 50 kHz to 0.10 Hz. EFM measurements were performed with applying potential perturbation signal with amplitude of 10 mV with two sine waves of 2 and 5 Hz. The intermodulation spectra contain current responses assigned for harmonical and intermodulation current peaks. The larger peaks were used to calculate the corrosion current density (j_{corr}), the Tafel slopes (β_c and β_a), and the causality factors CF2 & CF3 [31, 32].

Before each electrochemical experiment, the open circuit potential of the working electrode was measured as a function of time during 2 h, the time necessary to reach a quasi-stationary value for the open circuit potential.

All electrochemical experiments were carried out using Gamry PCI300/4 Potentiostat/Galvanostat/Zra analyzer, DC105 Corrosion software, EIS300 Electrochemical Impedance Spectroscopy software, EFM140 Electrochemical Frequency Modulation software, and Echem Analyst 5.21 for results plotting, graphing, data fitting and calculating.

Some of uncorroded and corroded samples were subjected to EDX analysis using model Oxford Link ISIS. Micrographs were made of same low alloy steel specimens using JEOL Scanning Electron Microscope (SEM) model T-200.

Results and discussion

Weight loss measurements

The weight loss (in mg cm^{-2}) of low alloy steel in 0.5 M HCl solutions devoid of and containing different concentrations (1.0 – 50 mM) of Tyr was studied as a function of immersion time in the range of temperature (20 – 60 °C). Figure 1, as a representative example, depicts results recorded at 20 °C. Similar results were obtained at 30 , 40 , 50 , and 60 °C. The slope of each line ($\text{mg cm}^{-2} \text{min}^{-1}$) represents the corrosion rate (v_w), see Table 1, of low alloy steel at the specified conditions.

The linear increase in the weight loss with time in the absence and presence of Tyr indicates that insoluble

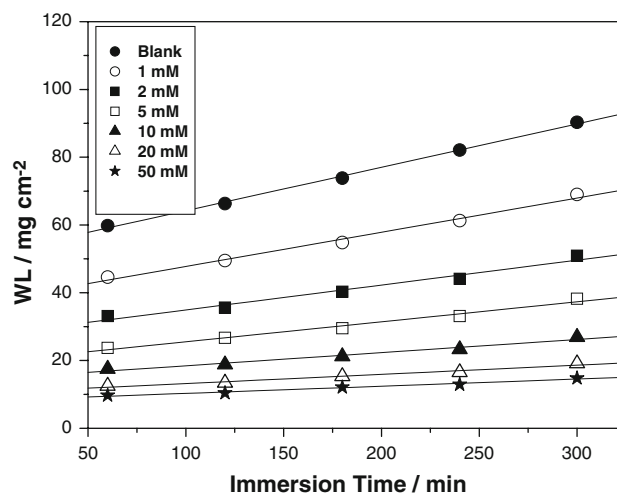


Fig. 1 Weight loss (in mg cm^{-2}) versus immersion time plots recorded for low alloy steel in 0.5 M HCl solutions devoid of and containing different concentrations (1.0 – 50 mM) of Tyr at 20 °C

surface films do not form on the electrode surface during steel corrosion in HCl solutions. This means that Tyr is first adsorbed on the electrode surface impeding corrosion either by merely blocking the reaction sites (anodic and cathodic) or by altering the mechanism of the anodic and cathodic processes [35]. It is obvious from Fig. 1 that the weight loss decreased (i.e., corrosion rate is suppressed), and therefore the corrosion inhibition strengthened, with increase in inhibitor concentration. This trend may result from the fact that adsorption and surface coverage increases with the increase in Tyr concentration; thus the surface is efficiently separated from the medium [36].

The inhibition efficiency values, I_w (%) (see also Table 1) were calculated for steel in 0.5 M HCl solutions containing various concentrations of Tyr as a function of temperature, using Eq. 1 [37–39]:

$$I_w (\%) = [1 - (\text{WL}/\text{WL}^0)] \times 100 \quad (1)$$

where WL^0 and WL are the weight losses of specimens without and with inhibitor, respectively.

It follows from Table 1 that, at a given temperature, the inhibition efficiency increases with increase in Tyr concentration, since more protonated Tyr molecules (TyrH^+), as will be seen, electrostatically adsorb on the electrode surface. It is seen that Tyr has inhibiting properties at all the studied temperatures and the values of I_w (%) decrease with temperature increase. This shows that the inhibitor has experienced a significant decrease in its protective properties with increase in temperature.

This decrease in the protective properties of the inhibitor with increase in temperature may be connected with two effects; a certain drawing of the adsorption–desorption equilibrium toward desorption (meaning that the strength of adsorption process decreases at higher temperatures) and

Table 1 Corrosion rates and inhibition efficiencies, I_w (%), obtained from weight loss measurements for low alloy steel in 0.50 M HCl solutions containing various concentrations of Tyr at different temperatures

| T (°C) | [Tyr] (mM) | Corrosion rate (mg cm ⁻² min ⁻¹) | I_w (%) |
|----------|------------|---|-----------|
| 20 | Blank | 0.414 | – |
| | 1.0 | 0.310 | 25.02 |
| | 2.0 | 0.227 | 45.20 |
| | 5.0 | 0.168 | 59.40 |
| | 10 | 0.120 | 71.10 |
| | 20 | 0.085 | 79.40 |
| | 50 | 0.067 | 83.92 |
| | 30 | Blank | 0.470 |
| 1.0 | | 0.366 | 22.13 |
| 2.0 | | 0.286 | 39.06 |
| 5.0 | | 0.230 | 51.02 |
| 10 | | 0.190 | 59.48 |
| 20 | | 0.110 | 76.49 |
| 50 | | 0.089 | 80.97 |
| 40 | | Blank | 0.524 |
| | 1.0 | 0.429 | 18.28 |
| | 2.0 | 0.370 | 29.53 |
| | 5.0 | 0.313 | 40.39 |
| | 10 | 0.274 | 47.68 |
| | 20 | 0.155 | 70.53 |
| | 50 | 0.118 | 77.48 |
| | 50 | Blank | 0.607 |
| 1.0 | | 0.519 | 14.58 |
| 2.0 | | 0.469 | 22.71 |
| 5.0 | | 0.413 | 32.05 |
| 10 | | 0.342 | 43.64 |
| 20 | | 0.204 | 66.42 |
| 50 | | 0.165 | 72.80 |
| 60 | | Blank | 0.689 |
| | 1.0 | 0.614 | 10.92 |
| | 2.0 | 0.556 | 19.36 |
| | 5.0 | 0.500 | 27.45 |
| | 10 | 0.441 | 36.04 |
| | 20 | 0.287 | 58.39 |
| | 50 | 0.206 | 70.09 |

roughening of the metal surface which results from enhanced corrosion. These results suggest that physical adsorption may be the type of adsorption of the inhibitor on the steel surface.

Polarization measurements

Figure 2 shows the potentiodynamic cathodic and anodic polarization curves recorded for low alloy steel in 0.5 M

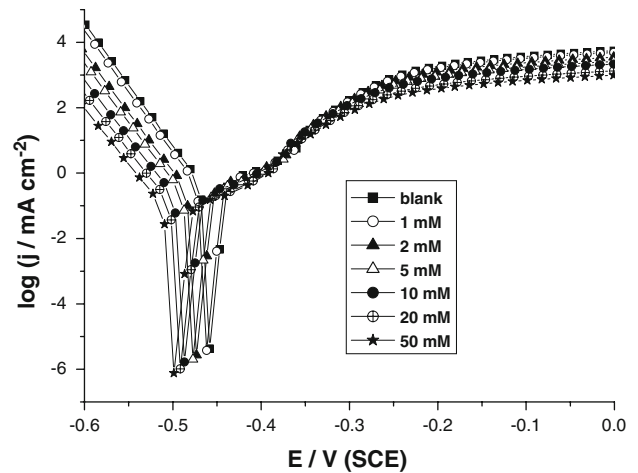


Fig. 2 Potentiodynamic cathodic and anodic polarization curves recorded for low alloy steel in 0.5 M HCl in the absence and presence of different concentrations of Tyr at a scan rate of 0.5 mV s⁻¹ at 30 °C

HCl in the absence and presence of different concentrations of Tyr at 30 °C. Similar plots were obtained for steel at the other studied temperatures. The curves infer that the presence of Tyr in the acid solution increases both the cathodic and anodic overpotentials. Tyr, therefore, exerted an efficient inhibitory effect both on anodic dissolution of the low alloy steel and on cathodic hydrogen evolution reaction. The cathodic overpotential, however, is suppressed to greater extents than the anodic one. Based on these results, Tyr can be considered as a mixed-type inhibitor with cathodic predominance. The inhibition function of this inhibitor is related to its adsorption and formation of barrier film on the alloy surface, preventing it from corrosion. Surface analysis using EDX/SEM examinations of the uninhibited and inhibited steel surfaces revealed the formation of such adsorbed protective film (see later).

Regarding to cathodic domains, it is obvious that the steel electrode immersed in this acid solution displays a typical cathodic region of Tafel behavior. In presence of various concentrations of Tyr, the cathodic polarization curves give rise to parallel Tafel lines (nearly constant cathodic Tafel slopes, β_c). These findings indicate that the hydrogen evolution reaction is activation-controlled and the addition of Tyr does not affect the mechanism of the corrosion process [40, 41]. This means that the inhibition of the hydrogen evolution reaction by Tyr occurs by simple adsorption mode and the mechanism is the same without and with inhibitor.

On the other hand, the anodic polarization curve does not display an extensive Tafel region, may be due to passivation and pitting (see the inflection in the anodic branch). The existence of passivation in conjunction with a

Table 2 Electrochemical kinetic parameters and inhibition efficiencies, I_{Tafel} (%), associated with Tafel polarization measurements for low alloy steel in 0.50 M HCl solutions containing various concentrations of Tyr at different temperatures

| T (°C) | [Tyr] (mM) | β_a (mV dec ⁻¹) | $-\beta_c$ (mV dec ⁻¹) | E_{corr} (mV) | j_{corr} (mA cm ⁻²) | I_{Tafel} (%) |
|----------|------------|-----------------------------------|------------------------------------|------------------------|--|------------------------|
| 20 | Blank | 85.00 | 59.00 | -456 | 0.165 | - |
| | 1.0 | 87.00 | 63.00 | -458 | 0.120 | 27.00 |
| | 2.0 | 89.00 | 57.00 | -464 | 0.088 | 46.88 |
| | 5.0 | 85.00 | 55.00 | -469 | 0.063 | 61.75 |
| | 10 | 88.00 | 58.00 | -475 | 0.045 | 73.00 |
| | 20 | 85.00 | 62.00 | -483 | 0.030 | 81.77 |
| | 50 | 87.00 | 64.00 | -491 | 0.024 | 85.23 |
| 30 | Blank | 86.00 | 55.00 | -459 | 0.200 | - |
| | 1.0 | 88.00 | 56.00 | -462 | 0.154 | 23.05 |
| | 2.0 | 85.00 | 55.00 | -473 | 0.116 | 42.00 |
| | 5.0 | 89.00 | 58.00 | -477 | 0.094 | 53.00 |
| | 10 | 88.00 | 62.00 | -487 | 0.076 | 62.12 |
| | 20 | 84.00 | 59.00 | -492 | 0.043 | 78.33 |
| | 50 | 84.00 | 57.00 | -499 | 0.035 | 82.45 |
| 40 | Blank | 85.00 | 59.00 | -461 | 0.260 | - |
| | 1.0 | 89.00 | 58.00 | -466 | 0.205 | 21.00 |
| | 2.0 | 91.00 | 60.00 | -477 | 0.177 | 32.00 |
| | 5.0 | 88.00 | 57.00 | -482 | 0.148 | 43.00 |
| | 10 | 87.00 | 60.00 | -493 | 0.131 | 49.44 |
| | 20 | 86.00 | 63.00 | -498 | 0.073 | 71.87 |
| | 50 | 86.00 | 56.00 | -507 | 0.055 | 79.00 |
| 50 | Blank | 86.00 | 55.00 | -510 | 0.305 | - |
| | 1.0 | 88.00 | 57.00 | -468 | 0.253 | 16.92 |
| | 2.0 | 89.00 | 60.00 | -479 | 0.230 | 24.65 |
| | 5.0 | 88.00 | 59.00 | -488 | 0.198 | 35.00 |
| | 10 | 86.00 | 58.00 | -499 | 0.165 | 46.00 |
| | 20 | 87.00 | 59.00 | -503 | 0.098 | 67.96 |
| | 50 | 83.00 | 61.00 | -511 | 0.076 | 75.00 |
| 60 | Blank | 88.00 | 56.00 | -465 | 0.368 | - |
| | 1.0 | 88.00 | 56.00 | -475 | 0.320 | 13.00 |
| | 2.0 | 89.00 | 57.00 | -484 | 0.288 | 21.81 |
| | 5.0 | 91.00 | 55.00 | -495 | 0.258 | 30.00 |
| | 10 | 87.00 | 59.00 | -505 | 0.224 | 39.00 |
| | 20 | 86.00 | 61.00 | -510 | 0.140 | 61.98 |
| | 50 | 89.00 | 63.00 | -517 | 0.099 | 73.00 |

dissolution reaction, due to pitting, does not result in a well-defined experimental anodic Tafel region. Therefore, due to absence of linearity in anodic branch, accurate evaluation of the anodic Tafel slope by Tafel extrapolation of the anodic branch is impossible [42, 43]. There is, therefore, an uncertainty and source error in the numerical values of the anodic Tafel slope (β_a), and may be in values of j_{corr} too, calculated by the software. For these reasons, the various electrochemical parameters associated with polarization measurements were evaluated by extrapolation of the linear cathodic Tafel regions and the calculated anodic Tafel lines, see more details in our previous study [29].

Table 2 collects the various electrochemical parameters as a function of Tyr concentration and temperature. The obtained j_{corr} values were introduced into Eq. 2 to get inhibition efficiencies, I_{Tafel} (%), as a function of Tyr concentration and temperature (see also Table 2):

$$I_{\text{Tafel}} (\%) = 100 \times [(j_{\text{corr}}^0 - j_{\text{corr}}) / j_{\text{corr}}^0] \quad (2)$$

where j_{corr}^0 and j_{corr} are the corrosion current densities for uninhibited and inhibited solutions, respectively. As it can be seen the values of j_{corr} , at any given temperature, decrease with increase in Tyr concentration. Inhibition efficiency values also enhance with Tyr concentration. These findings confirm the inhibiting ability of Tyr toward steel corrosion

in HCl solutions at any given temperature in the studied temperature range. On the other hand, the j_{corr} values increase, while those of I_{Tafel} (%) decrease, and therefore the rate of corrosion is enhanced, with increase in temperature, confirming the occurrence of physical adsorption.

Impedance measurements

Effect of inhibitor concentration and temperature

In this study, complex-plane impedance plots were recorded for steel in 0.5 M HCl solutions without and with various concentrations of Tyr in the temperature range (20–60 °C) at the respective corrosion potentials. Figure 3, as an example, shows the results recorded at 50 °C. Similar plots were obtained at the other temperatures. All Nyquist plots presented in Fig. 3 are depressed charge-transfer semicircle, which is attributed to the time constant of charge-transfer and double-layer capacitance [44–46].

Depressed semicircles are usually obtained for practical electrode/solution interface, which has been known to be associated with the roughness of electrode surface. It is well known that the corrosion of steel in the HCl solutions increases the roughness of the electrode surface (see later the SEM images). This semicircle intersects the real axis at high frequencies to give a value of about 1.25 Ω cm² for the resistance of the solution (R_s) enclosed between the working electrode and the counter electrode. It is clear that the shapes of the impedance plots for inhibited electrodes are not substantially different from those of uninhibited electrodes. The presence of the inhibitor increases the impedance but does not change other aspects of the behavior. These results support the results of polarization measurements that the inhibitor does not alter the electrochemical reactions responsible for corrosion. It inhibits corrosion primarily through its adsorption on the metal surface.

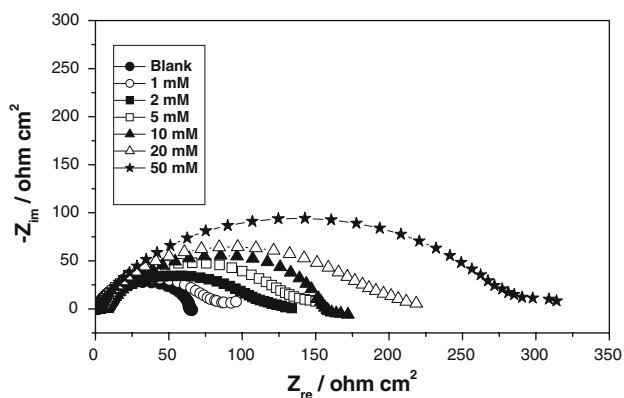


Fig. 3 Complex-plane impedance plots recorded for low alloy steel in 0.5 M HCl in the absence and presence of different concentrations of Tyr at the respective corrosion potentials at 50 °C

Equivalent circuit and calculation of the impedance parameters

To determine the impedance parameters (see Table 3) of the steel electrode in these solutions, the measured impedance data were analyzed based on the electric equivalent circuit presented in our previous study [29]. One constant phase element (CPE) is substituted for the capacitive element to give a more accurate fit [47], as the obtained capacitive loop is a depressed semi-circle rather

Table 3 Electrochemical kinetic parameters obtained by EIS technique, together with the inhibition efficiency (I_z (%)) for low alloy steel in aerated 0.50 M HCl solutions containing various concentrations of Tyr at different temperatures

| T (°C) | [Tyr] (mM) | C_{dl} ($\mu\text{F cm}^{-2}$) | R_{ct} ($\Omega \text{ cm}^2$) | I_z (%) |
|--------|------------|------------------------------------|------------------------------------|-----------|
| 20 | Blank | 793.9 | 88.29 | – |
| | 1.0 | 588.2 | 121.10 | 27.09 |
| | 2.0 | 473.9 | 148.30 | 40.47 |
| | 5.0 | 322.1 | 214.70 | 58.88 |
| | 10 | 285.5 | 259.00 | 65.91 |
| | 20 | 237.8 | 303.10 | 70.87 |
| 30 | Blank | 956.4 | 82.81 | – |
| | 1.0 | 745.1 | 107.10 | 22.68 |
| | 2.0 | 613.5 | 135.60 | 38.93 |
| | 5.0 | 453.6 | 171.50 | 51.71 |
| | 10 | 385.3 | 204.80 | 59.57 |
| | 20 | 331.7 | 251.50 | 67.07 |
| 40 | Blank | 1094.7 | 70.00 | – |
| | 1.0 | 871.2 | 90.62 | 22.75 |
| | 2.0 | 761.2 | 102.00 | 31.37 |
| | 5.0 | 553.4 | 132.70 | 47.25 |
| | 10 | 462.7 | 172.00 | 59.30 |
| | 20 | 411.5 | 185.70 | 62.30 |
| 50 | Blank | 1238.5 | 60.17 | – |
| | 1.0 | 1033.5 | 72.50 | 17.01 |
| | 2.0 | 891.3 | 86.77 | 30.66 |
| | 5.0 | 673.5 | 113.60 | 47.03 |
| | 10 | 547.1 | 132.20 | 54.49 |
| | 20 | 493.5 | 157.00 | 61.68 |
| 60 | Blank | 1421.6 | 44.16 | – |
| | 1.0 | 1229.3 | 51.00 | 13.41 |
| | 2.0 | 1089.7 | 56.61 | 21.99 |
| | 5.0 | 847.8 | 76.25 | 42.09 |
| | 10 | 699.3 | 94.13 | 53.09 |
| | 20 | 617.5 | 100.30 | 55.97 |
| | 50 | 417.2 | 147.70 | 70.10 |

than regular one. The CPE is a special element whose immittance value is a function of the angular frequency (ω), and whose phase is independent of the frequency. Its admittance and impedance are, respectively, expressed as:

$$Y_{\text{CPE}} = Y_0 (j\omega)^n \quad (3)$$

and

$$Z_{\text{CPE}} = (1/Y_0) [(j\omega)^n]^{-1} \quad (4)$$

where Y_0 is the magnitude of the CPE, j is the imaginary number ($j^2 = -1$), α is the phase angle of the CPE and $n = \alpha/(\pi/2)$. The factor n is an adjustable parameter that usually lies between 0.50 and 1.0 [48, 49]. The CPE describes an ideal capacitor when $n = 1$. Values of α are usually related to the roughness of the electrode surface. The smaller value of α , the higher the surface roughness [48–50]. A good fit with this model was obtained with our experimental data.

The point of intersection between the capacitive loop and the real axis at low frequency values represents ($R_s + R_{\text{ct}}$) [51]. To obtain C_{dl} , the frequency (f_{max}) at which the imaginary component of the impedance is maximal was found and used in Eq. 5:

$$C_{\text{dl}} = 1/2\pi f_{\text{max}} R_{\text{ct}} \quad (5)$$

Based on Table 3, the values of R_{ct} increase with increase in Tyr concentration, while the C_{dl} values tend to decrease. The decrease in the C_{dl} values with increase in Tyr concentration may be due to the inhibitor adsorption and formation of a protective layer on the electrode surface [52]. The adsorption of Tyr on the electrode surface decreases its electrical capacity because they displace the water molecules and other ions originally adsorbed on the surface.

On the other hand, the temperature increase leads to an essential decrease of R_{ct} and an increase of C_{dl} values which on one hand may be attributed to the corrosion rate increase and on the other hand to the probable partial desorption of the inhibitor under these conditions. But the concentration of the inhibitor is high to sustain an inhibiting adsorption layer at a given temperature. It may be assumed that the density of the inhibitor adsorbed layer within outer Helmholtz layer (OHL) decreases, while the diffuse part of the double electrical layer increases with temperature.

The R_{ct} values were used to calculate the inhibition efficiency, I_Z (%), at different Tyr concentrations and temperatures (see also Table 3), using Eq. 6 [53]:

$$I_Z(\%) = 100 \times [(R_{\text{ct}} - R_{\text{ct}}^0)/R_{\text{ct}}] \quad (6)$$

where R_{ct}^0 and R_{ct} are the charge-transfer resistances for uninhibited and inhibited solutions, respectively. It is apparent that the inhibition efficiency increases with increase in inhibitor concentration. It is worth noting from

Table 3 that the inhibition efficiencies obtained from impedance measurements are comparable and run parallel with those obtained from weight loss (Table 1) and Tafel polarization (Table 2) measurements.

Electrochemical frequency modulation measurements

EFM is a nondestructive corrosion measurement technique that can directly give values of the corrosion current without prior knowledge of Tafel constants. Like EIS, it is a small signal ac technique. Unlike EIS, however, two sine waves (at different frequencies) are applied to the cell simultaneously. Because current is a nonlinear function of potential, the system responds in a nonlinear way to the potential excitation. The current response contains not only the input frequencies, but also contains frequency components which are the sum, difference, and multiples of the two input frequencies. The two frequencies may not be chosen at random. They must both be small, integer multiples of a base frequency that determines the length of the experiment. Figure 4 shows representative examples for the intermodulation spectra obtained from EFM measurements at 20 °C. Similar plots were obtained at the other studied temperatures. Each spectrum is a current response as a function of frequency. Corrosion kinetic parameters listed in Table 4, were calculated from the EFM technique using the following equations:

$$i_{\text{corr}} = \frac{i_{\omega}^2}{\sqrt{48(2i_{\omega}i_{3\omega} - i_{2\omega})}} \quad (7)$$

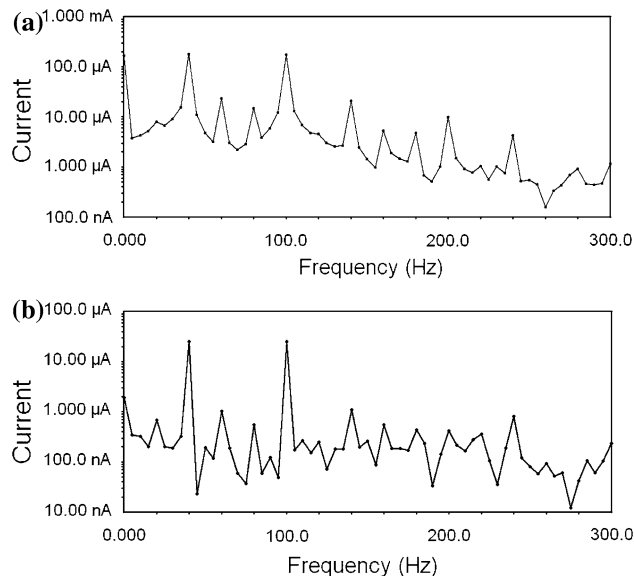


Fig. 4 Intermodulation spectra recorded, using EFM measurements, for low alloy steel in 0.5 M HCl solution **a** without and **b** with 50 mM Tyr at 20 °C

Table 4 Electrochemical kinetic parameters obtained by EFM technique, and the inhibition efficiency values (I_{EFM} (%)), recorded for low alloy steel in aerated 0.50 M HCl solutions without and with various concentrations of Tyr at different temperatures

| T (°C) | [Tyr] (mM) | β_a (mV dec ⁻¹) | $-\beta_c$ (mV dec ⁻¹) | i_{corr} (mA cm ⁻²) | I_{EFM} (%) | CF(2) | CF(3) |
|----------|------------|-----------------------------------|------------------------------------|-----------------------------------|---------------|-------|-------|
| 20 | Blank | 91.00 | 65.00 | 0.173 | – | 1.87 | 2.88 |
| | 1.0 | 89.00 | 64.00 | 0.126 | 27.23 | 1.92 | 2.93 |
| | 2.0 | 88.00 | 63.00 | 0.097 | 44.14 | 1.88 | 2.94 |
| | 5.0 | 93.00 | 61.00 | 0.070 | 59.27 | 1.85 | 2.88 |
| | 10 | 88.00 | 65.00 | 0.051 | 70.43 | 1.95 | 2.89 |
| | 20 | 93.00 | 59.00 | 0.036 | 79.16 | 2.03 | 2.97 |
| | 50 | 92.00 | 61.00 | 0.029 | 83.19 | 1.97 | 2.99 |
| 30 | Blank | 89.00 | 59.00 | 0.219 | – | 2.22 | 2.98 |
| | 1.0 | 91.00 | 62.00 | 0.169 | 23.00 | 2.04 | 2.95 |
| | 2.0 | 92.00 | 61.00 | 0.139 | 36.51 | 1.93 | 2.97 |
| | 5.0 | 91.00 | 57.00 | 0.109 | 50.11 | 1.95 | 2.95 |
| | 10 | 90.00 | 59.00 | 0.093 | 57.38 | 1.95 | 2.94 |
| | 20 | 88.00 | 60.00 | 0.056 | 74.25 | 1.98 | 2.91 |
| | 50 | 91.00 | 61.00 | 0.043 | 80.40 | 1.88 | 2.89 |
| 40 | Blank | 89.00 | 57.00 | 0.266 | – | 1.65 | 3.26 |
| | 1.0 | 92.00 | 58.00 | 0.224 | 15.84 | 1.89 | 3.07 |
| | 2.0 | 91.00 | 59.00 | 0.180 | 32.36 | 1.88 | 3.05 |
| | 5.0 | 93.00 | 61.00 | 0.153 | 42.38 | 1.69 | 2.99 |
| | 10 | 88.00 | 62.00 | 0.131 | 50.86 | 1.98 | 2.98 |
| | 20 | 87.00 | 63.00 | 0.083 | 68.73 | 1.99 | 2.97 |
| | 50 | 91.00 | 59.00 | 0.061 | 76.96 | 1.93 | 2.95 |
| 50 | Blank | 83.00 | 59.00 | 0.316 | – | 1.89 | 3.26 |
| | 1.0 | 88.00 | 63.00 | 0.258 | 18.50 | 1.85 | 3.11 |
| | 2.0 | 89.00 | 61.00 | 0.244 | 22.76 | 1.82 | 3.05 |
| | 5.0 | 91.00 | 60.00 | 0.210 | 33.54 | 1.89 | 2.86 |
| | 10 | 92.00 | 58.00 | 0.184 | 41.92 | 1.94 | 2.88 |
| | 20 | 91.00 | 59.00 | 0.109 | 65.38 | 1.97 | 2.97 |
| | 50 | 89.00 | 63.00 | 0.086 | 72.84 | 1.98 | 2.96 |
| 60 | Blank | 82.00 | 61.00 | 0.380 | – | 1.91 | 3.26 |
| | 1.0 | 87.00 | 63.00 | 0.329 | 13.51 | 1.95 | 2.98 |
| | 2.0 | 88.00 | 60.00 | 0.303 | 20.36 | 1.93 | 2.94 |
| | 5.0 | 89.00 | 58.00 | 0.288 | 24.18 | 1.90 | 2.90 |
| | 10 | 91.00 | 59.00 | 0.233 | 38.58 | 1.97 | 2.88 |
| | 20 | 92.00 | 62.00 | 0.154 | 59.39 | 1.88 | 2.97 |
| | 50 | 93.00 | 58.00 | 0.116 | 69.50 | 1.93 | 2.95 |

$$\beta_a = \frac{i_\omega U_0}{2i_{2\omega} + 2\sqrt{3}\sqrt{2i_{3\omega}i_\omega - i_{2\omega}^2}} \tag{8}$$

$$\beta_a = \frac{i_\omega U_0}{2\sqrt{3}\sqrt{2i_{3\omega}i_\omega - i_{2\omega}^2} - 2i_{2\omega}} \tag{9}$$

$$\text{Casuality factor (2)} = \frac{i_{\omega_2 \pm \omega_1}}{i_{2\omega_1}} = 2.0 \tag{10}$$

$$\text{Casuality factor (3)} = \frac{i_{2\omega_2 \pm \omega_1}}{i_{3\omega_1}} = 3.0 \tag{11}$$

where i is the instantaneous current density at the working electrode measured at frequency ω and U_0 is the amplitude of the sine wave distortion. The obtained i_{corr} values were

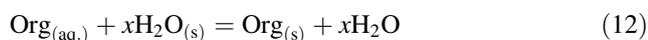
introduced into Eq. 2 to calculate the inhibition efficiency, I_{EFM} (%) of Tyr as a function of its concentration (see also Table 4).

Inspections of Table 4 infer that addition of increasing concentrations of Tyr decreases the corrosion current density, $(i_{corr})_{EFM}$, indicating that Tyr inhibits acid corrosion of steel through adsorption. The calculated inhibition efficiencies also enhance with Tyr concentration. The great strength of the EFM is the causality factors which serve as an internal check on the validity of the EFM measurement [31, 32]. With the causality factors, the experimental EFM data can be verified. The causality factors in Table 4 indicate that the measured data are of good quality. The

standard values for CF-2 and CF-3 are 2.0 and 3.0, respectively. Results obtained from the EFM technique are in agreement with those recorded with Tafel extrapolation, impedance and weight loss methods. These findings confirm validation of corrosion rates measured by EFM technique.

Adsorption isotherms

The steel corrosion inhibition by Tyr can be explained by the adsorption of Tyr on the steel surface so as to impede the electron transfer. The adsorption of inhibitor molecules from aqueous solutions can be regarded as a quasi-substitution process between the organic compound in the aqueous phase $\text{Org}_{(\text{aq})}$ and water molecules at the electrode surface, $\text{H}_2\text{O}_{(\text{s})}$



where x , the size factor, is the number of water molecules displaced by one molecule of organic inhibitor. Adsorption isotherms are very important in determining the mechanism of organo-electrochemical reactions [54]. Most of these isotherms are of the general form:

$$f(\theta, x) \exp(2a\theta) = KC \quad (13)$$

where $f(\theta, x)$ is the configurational factor which depends upon the physical model and the assumptions underlying the derivation of the isotherm, θ the surface coverage degree, C the inhibitor concentration in the bulk of solution, “ a ” the lateral interaction term describing the molecular interactions in the adsorption layer and the heterogeneity of the surface and is a measure for the steepness of the adsorption isotherm, K the adsorption–desorption equilibrium constant.

The values of surface coverage ($\theta = I(\%)/100$) to different concentrations of Tyr, obtained from weight loss, polarization, and impedance measurements in the range of temperature (20–60 °C), have been used to explain the best isotherm to determine the adsorption process. In the range of temperature studied, the best correlation between the experimental results, obtained from the three techniques, and the isotherm functions was obtained using Temkin adsorption isotherm (Eq 14).

$$\exp(2a\theta) = KC \quad (14)$$

Figure 5 represents, as an example, fitting of the data obtained from Tafel extrapolation method for steel in 0.5 M HCl solutions containing various concentrations of Tyr to Temkin isotherm at different temperatures (20–60 °C). The isotherms’ parameters (K and a) and the free energies of the inhibitor adsorption, calculated from Eq 15 [55], are shown in Tables 5 and 6, respectively.

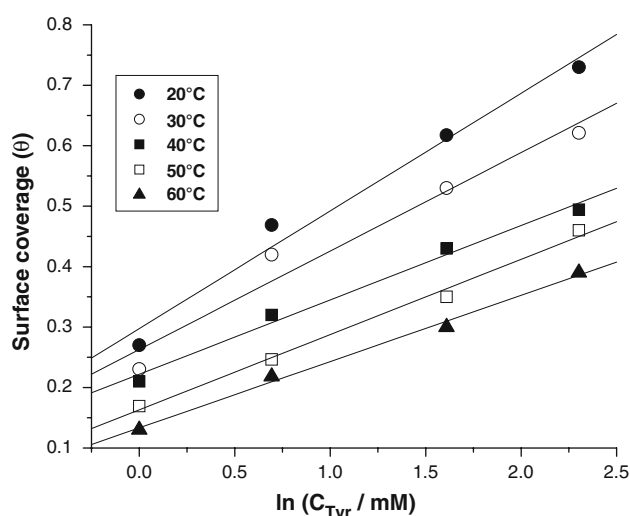


Fig. 5 Fitting of the data obtained from Tafel extrapolation method for steel in 0.5 M HCl solutions containing various concentrations of Tyr to Temkin isotherm at different temperatures (20–60 °C)

Table 5 Values of “ K ” and “ a ” obtained from fitting Tafel polarization data with Temkin adsorption isotherm at various temperatures

| T (K) | K | a |
|---------|------|------|
| 293 | 7560 | 0.75 |
| 303 | 6700 | 0.73 |
| 313 | 5950 | 0.71 |
| 323 | 5120 | 0.68 |
| 333 | 3935 | 0.65 |

Table 6 Thermodynamic parameters of Tyr adsorption process obtained from Tafel polarization measurements for low alloy steel in 0.50 M HCl solutions containing various concentrations of Tyr at 30 °C

| [Tyr] (mM) | $-\Delta G_{\text{ads}}$ (kJ mol ⁻¹) | $-\Delta H_{\text{ads}}$ (kJ mol ⁻¹) | ΔS_{ads} (J mol ⁻¹ K ⁻¹) |
|------------|--|--|--|
| 1.0 | 18.75 | 9.71 | 63.51 |
| 2.0 | 21.00 | 11.41 | 51.25 |
| 5.0 | 24.77 | 14.53 | 32.77 |
| 10 | 26.55 | 16.05 | 11.53 |
| 20 | 28.00 | 19.00 | 3.22 |
| 50 | 29.95 | 21.12 | -2.21 |

$$K = (1/55.5) \exp(-\Delta G_{\text{ads}}^{\circ}/RT) \quad (15)$$

where $\Delta G_{\text{ads}}^{\circ}$ is the free energy of adsorption, 55.5 the concentration of water in the solution in mol L⁻¹, R the universal gas constant, T the thermodynamic temperature. It follows from the theory of adsorption from solutions [55] that:

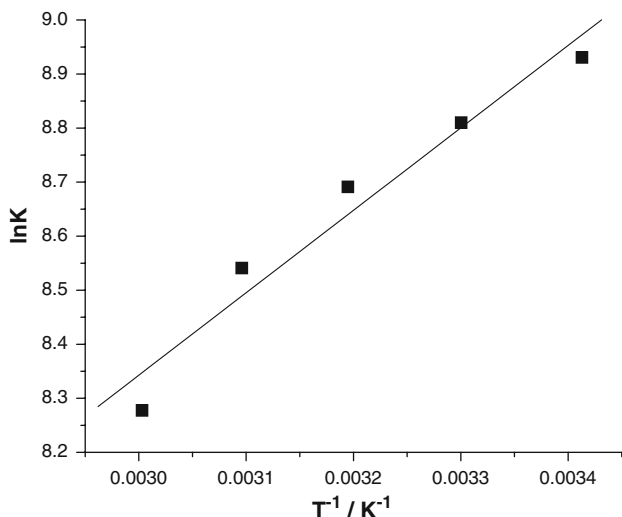


Fig. 6 Linear relation between $\ln K$ and $(1/T)$ for steel in 0.5 M HCl solutions containing various concentrations of Tyr

$$(d \ln K / dT)_\theta = -\Delta H_{\text{ads}}^0 / RT^2 \tag{16}$$

where ΔH_{ads}^0 is the isosteric enthalpy of adsorption. The integrated version of the Van't Hoff equation:

$$\ln K = -\Delta H_{\text{ads}}^0 / RT + \text{constant} \tag{17}$$

may be used to determine ΔH_{ads}^0 . The slopes of the lines, shown in Fig. 6, depict the linear relation between $\ln K$ and $(1/T)$ at a given surface coverage. These slopes, multiplied by R , give the values of ΔH_{ads}^0 shown in Table 6. The values of the entropy change of the inhibitor adsorption (ΔS_{ads}^0), also listed in Table 6, were calculated from Eq. 18 [53]:

$$\Delta G_{\text{ads}}^0 = \Delta H_{\text{ads}}^0 - T\Delta S_{\text{ads}}^0 \tag{18}$$

It follows from Table 5 that the values of K are relatively low and decrease with an increase in temperature. Large values of K mean better inhibition efficiency of the inhibitor, i.e., strong electrical interaction between the double-layer existing at the phase boundary and the adsorbing inhibitor molecules. Small values of K , however, compromise that such interactions between adsorbing inhibitor molecules and the metal surface are weaker, indicating that the inhibitor molecules are easily removable by the solvent molecules from the surface. These results confirm the suggestion that this inhibitor is physically adsorbed on the metal surface and the strength of the adsorption decreases with temperature. Small and positive values of “ a ” would indicate the existence of weak lateral forces of attraction between adsorbate molecules in the adsorption layer [55].

From Table 6, the negative values of ΔG_{ads}^0 ensure the spontaneity of the adsorption process and stability of the adsorbed layer on the electrode surface. Generally, values

of ΔG_{ads}^0 lower than -40 kJ mol^{-1} are consistent with the electrostatic interaction between the charged molecules and the charged metal (physisorption); those around -50 kJ mol^{-1} or higher involve charge sharing or charge transfer from organic molecules to the metal surface to form a coordinate type of bond (chemisorption) [56, 57]. In this study, the calculated values of ΔG_{ads}^0 are lower than -40 kJ mol^{-1} . These findings confirm results obtained from chemical and electrochemical measurements that the adsorption mechanism of Tyr on steel surface was typical of physisorption.

The negativity of the enthalpy (Table 6) means that heat is released from the adsorption process. Generally, an exothermic adsorption process signifies either physisorption or chemisorption, while endothermic process is attributable unequivocally to chemisorption [58]. In an exothermic process, physisorption is distinguished from chemisorption by considering the absolute value of adsorption enthalpy. Typically, the enthalpy of a physisorption process is lower than $41.86 \text{ kJ mol}^{-1}$, while that of a chemisorption process approaches 100 kJ mol^{-1} [58, 59].

In this study, the absolute values of enthalpy are low approaching those typical of physisorption (see Table 6). The absolute value of the adsorption enthalpy, $|\Delta H_{\text{ads}}^0|$, increases with the increase in surface coverage due to the attractive interaction between the adsorbed molecules indicating the validity of the Temkin model [55]. The origin of the attractive forces is most probably the dipole-dipole interaction occurring between the neighboring adsorbed molecules [60].

Table 6 clearly shows that the values of ΔS_{ads}^0 decrease with increasing inhibitor concentration. The entropy changes can be explained in terms of displacement of the H_2O molecules from the surface into the hydrogen-bonded aqueous solution and adsorption of inhibitor molecules at the surface from their surface-active positions in the solution phase [59].

Thermodynamic activation functions of the corrosion process

Further insight into the adsorption mechanism is offered by considering the thermodynamic functions for the steel dissolution in HCl solutions in the absence and presence of various concentrations of the inhibitor. These thermodynamic functions were obtained by applying the Arrhenius and the transition-state equations [60].

$$\ln(\text{rate}) = -(E_a^0 / RT) + \text{constant} \tag{19}$$

$$\text{rate} = (RT/Nh) \exp(\Delta S_a^0 / R) \exp(-\Delta H_a^0 / RT) \tag{20}$$

where E_a^0 is the apparent activation energy, ΔS_a^0 the apparent entropy of activation, ΔH_a^0 the apparent enthalpy

of activation, h Plank's constant, and N the Avogadro's number. Arrhenius and Transition-state plots obtained from chemical and electrochemical methods tested here were constructed for steel in 0.5 M HCl solutions without and with various concentrations of Tyr in the range of temperature (20–60 °C).

Rates of corrosion, v , (expressed in mm year^{-1}), see Eq. 21 [30], obtained from Tafel extrapolation method are depicted in Figs. 7 and 8 in the form of Arrhenius and Transition-state plots, respectively.

$$v \text{ (mm year}^{-1}\text{)} = 3.28 \times j_{\text{corr}} \times (M/nd) \quad (21)$$

where M is the atomic weight of Fe (55.85 g), n the number of electrons transferred in the corrosion reaction ($n = 2$),

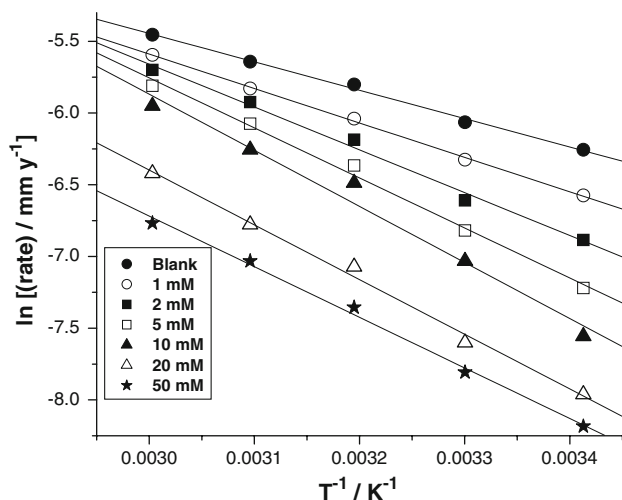


Fig. 7 Arrhenius plots obtained from Tafel extrapolation method for steel in 0.5 M HCl solutions containing various concentrations of Tyr

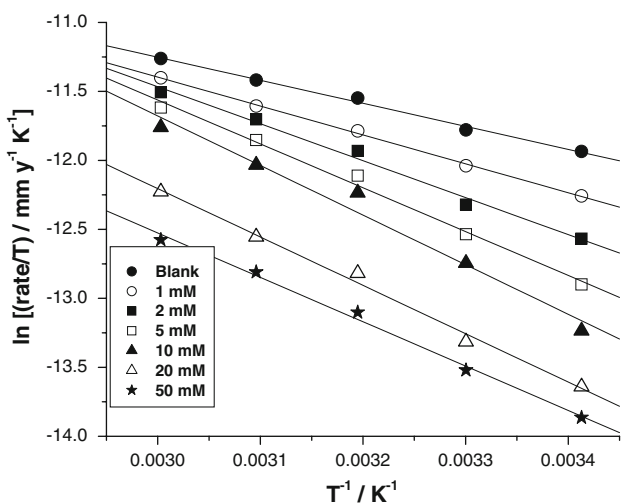


Fig. 8 Transition state plots obtained from Tafel extrapolation method for steel in 0.5 M HCl solutions containing various concentrations of Tyr

Table 7 Thermodynamic activation parameters associated with Tafel polarization measurements for low alloy steel in 0.50 M HCl solutions without and with various concentrations of Tyr

| [Tyr] (mM) | E_a (kJ mol^{-1}) | ΔH_a (kJ mol^{-1}) | $-\Delta S_a$ ($\text{J mol}^{-1} \text{K}^{-1}$) |
|------------|--------------------------------|---------------------------------------|---|
| Blank | 16.45 | 13.88 | 249.59 |
| 1.0 | 19.95 | 17.41 | 240.11 |
| 2.0 | 24.83 | 22.28 | 226.14 |
| 5.0 | 29.01 | 26.43 | 214.50 |
| 10 | 32.50 | 29.89 | 205.02 |
| 20 | 31.71 | 29.15 | 211.67 |
| 50 | 29.35 | 26.74 | 221.57 |

and d the density of Fe (7.88 g cm^{-3}). The values of these thermodynamic activation functions were calculated from Arrhenius and Transition state-plots and listed in Table 7.

The decrease of I (%) values with temperature increase (see Tables 1, 2, 3, and 4) and the higher values of E_a^0 in presence of Tyr than in its absence (Table 7) can be interpreted as an indication of physisorption. A general increase in activation energy with increase in inhibitor concentration is observed. This increase in E_a^0 with inhibitor concentration indicates that the energy barrier for the corrosion interaction is also increased [61–63]. This means that the corrosion reaction will be further pushed to the surface sights that are characterized by progressively higher values of E_a^0 as the concentration of the inhibitor in the solution becomes larger.

The positive sign of the enthalpy reflects the endothermic nature of the steel dissolution process. Negative values of the entropy imply that the activated complex in the rate-determining step represents an association rather than a dissociation step, meaning that a decrease in disordering takes place on going from reactants to the activated complex.

SEM and EDX examinations

Figure 9 shows a series of the SEM images for a polished steel sample (image a), a corroded steel sample (image b), and inhibited samples under various conditions (images c–e). These SEM images were obtained after immersing the tested sample for 5 and 12 h in 0.5 M HCl solutions without and with 5.0 and 20 mM Tyr. A rough-corroded surface was noticed for steel immersed in Tyr–0.5 M HCl free solution (image b). In case of steel immersed in 0.5 M HCl with 5.0 and 20 mM Tyr (images c and d, respectively) the corroded areas obviously diminished with increase in Tyr concentration, compare again between images c and d). This is obviously due to inhibitor adsorption on the corroded areas.

Finally, a smooth surface was noticed when the immersion time is increased, at a fixed Tyr concentration (20 mM), from 5 h (image d) to 12 h (image e) and it is

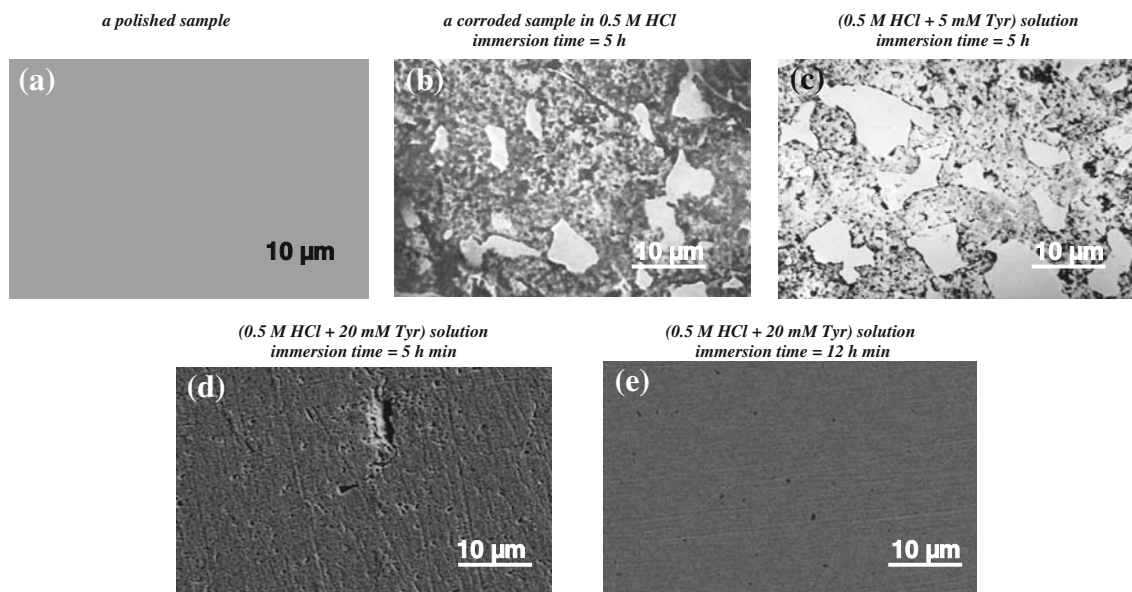


Fig. 9 SEM images recorded for a polished steel sample (image **a**), a steel sample corroded in 0.5 M HCl solution (image **b**) and inhibited samples under various conditions (images **c–e**); see details on each image

easily comparable with the polished surface (image **a**). It seems that surface coverage obviously increases with increase in Tyr concentration and immersion time, since more TyrH⁺ cations are expected, as will be seen, to electrostatically adsorb.

In order to confirm SEM examinations that a protective surface film of inhibitor is formed at the electrode surface, some EDX examinations were carried out (see Fig. 10). This figure presents the EDX spectra recorded for low alloy steel samples exposed for 5 h in 0.50 M HCl solutions (**a**) without and with, (**b**) 5.0, and (**c**) 20 mM Tyr. In absence of Tyr, the EDX spectra show the characteristics peaks of the elements constituting the low alloy steel sample.

In presence of increased concentrations of Tyr (Fig. 10**b** and **c**), the EDX spectra did not show additional lines. However, the oxygen signal is significantly enhanced. This enhancement in oxygen signal is due to the oxygen atoms of the adsorbed Tyr molecules. The intensity of the oxygen signal increases when Tyr concentration is increased from 5.0 to 20 mM, since more inhibitor molecules adsorb on the electrode surface. Same spectra also show that the iron lines observed in the presence of inhibitor are considerably suppressed relative to those observed in blank solution (Fig. 10**a**), and this suppression increases with increasing Tyr concentration. The suppression of the iron lines, therefore, occurs because of the overlying inhibitor film.

This observation indicates that there is an adsorbed layer formed and protects the electrode surface after immersion in the acid containing Tyr. The protective nature of this film is reflected in the inhibition efficiency values obtained from the chemical and electrochemical methods.

Therefore, SEM and EDX examinations of the electrode surface support the results obtained from chemical and electrochemical methods that Tyr is a good inhibitor for low alloy steel in HCl solutions.

Mechanism of adsorption

It is well known that amino acids present in its protonated form in acidic solutions. Thus in HCl solution, Tyr forms its hydrochloride, or more specifically, Tyr exists as a moiety of cationic form, namely TyrH⁺ and Cl⁻ ion. Based on chemical and electrochemical studies performed here, the HCl corrosion of steel was retarded by the presence of Tyr. Thus, the inhibition mechanism involves blockage of the active sites on the electrode surface by the inhibitor molecules via adsorption. In general, the phenomenon of adsorption is influenced by the nature and surface charge of the metal and by the chemical structure of inhibitors.

The surface charge of the metal is due to the electrical field which emerges at the interface on immersion in the electrolyte. It can be determined according to Antropov et al. [64] by comparing the potential of zero charge (PZC) and the stationary potential of the metal in the corresponding medium. As PZC corresponds to a state at which the surface is free from charges, at the stationary (corrosion) potential the metal surface will be positively or negatively charged. Hence, it is necessary to have reliable data about PZC.

In our previous study [65, 66], capacitance measurements as a function of applied potential showed that the steel surface is positively charged in HCl solutions at the

Fig. 10 EDX spectra recorded for steel immersed for 5 h in 0.5 M HCl solutions **a** without inhibitor (*blank*) and with **b** 5.0 mM Tyr, or **c** 50 mM Tyr at 30 °C

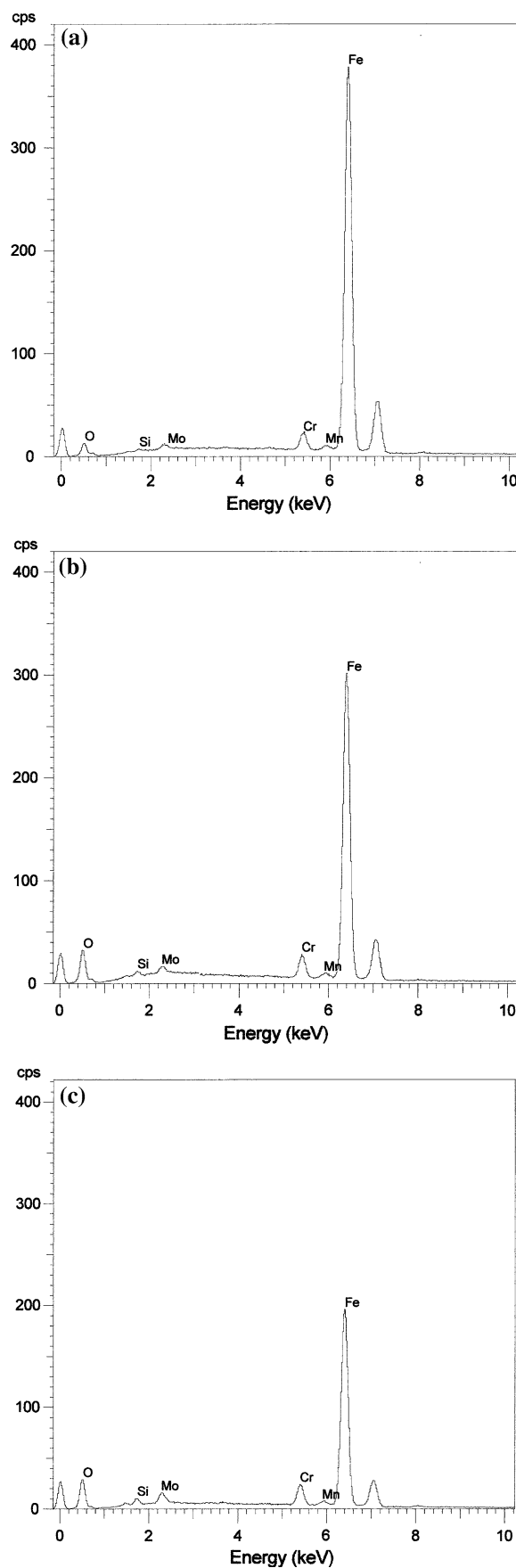
free corrosion potential. Based on these observations, the mechanism of adsorption of these amino acids on iron surface in HCl solutions is quite clear. Cl^- ions first adsorbed at the electrode/solution interface at the corrosion potential through electrostatic attraction force due to the excess positive charge at the this interface. This process changes the charge of the solution side of the interface from positive to negative, and thus facilitating physical adsorption of the inhibitors' cations.

Thus, cations of these amino acids are able to electrostatically adsorb on the electrode surface covered with primary adsorbed Cl^- ions. It is obvious, therefore, that Cl^- ions promote the physical adsorption of cations on the electrode surface. On the other hand, the resultant cationic species can be adsorbed directly on cathodic sites and retard the rate of the hydrogen evolution reaction. This may be responsible for the observed cathodic inhibiting effect of Tyr.

Based on the results presented here, temperature effect and thermodynamics of adsorption did not confirm chemical adsorption. However, it is not wise to ignore the possibility of adsorption via coordinate bonds (see later). We believe that physical adsorption may be followed by chemical adsorption, particularly after a long immersion time. We would say, in addition to the physical adsorption, there should be chemical adsorption owing to the coordinate bonds that may be formed between the lone electron pairs of the unprotonated N and the empty orbits of Fe atoms which enhanced the combination intensity between the inhibitor molecule and electrode surface.

A contribution from the carboxylic group (π -bond of the $\text{C}=\text{O}$ and lone pair of electrons on the O atom in the $-\text{OH}$ link) may also occur. Moreover, adsorption via the delocalized p-electrons of the benzene ring and the electron pairs on the oxygen atom of the phenolic $-\text{OH}$ group also takes place. Indeed, the presence of $-\text{Ph}-\text{OH}$ in molecular structure of Tyr provokes an increase of the inhibition efficiency. The group $-\text{Ph}-\text{OH}$ is a donor of electron and it offers itself the possibility to be a center of adsorption beside the nitrogen and oxygen atoms.

Perhaps, the adsorbed nitrogen and oxygen atoms are oriented with the benzene ring structure parallel to the metal surface (due to aromaticity of Tyr molecule). This mode of adsorption suggests that the adsorbed Tyr molecule covers a large area, thereby inhibiting steel corrosion effectively, even at low concentrations (i.e., low surface coverage). This may explain why Tyr is better than Glycine, see our previous study [29], in inhibiting corrosion of this low alloy steel in HCl solutions.



Conclusion

In this study, Tyr was tested as an environmentally friendly inhibitor for low chromium alloy steel corrosion in 0.5 M HCl solution. For this purpose, chemical (weight loss) and electrochemical (Tafel polarization, impedance, and EFM) methods were used. According to the collected results, Tyr is a good inhibitor in 0.5 M HCl. Polarization curves showed that the inhibitor is a mixed-type one with cathodic predominance. The inhibition efficiency increased with increase in inhibitor concentration, but decreased with temperature. These findings indicate that (Tyr) physisorbs on the electrode surface.

Activation energies have been calculated in the absence and presence of various concentrations of (Tyr) by measuring the temperature dependence of the corrosion rate obtained from Tafel extrapolation method. The adsorptive behavior of (Tyr) on the steel surface follows Temkin-type isotherm. The recorded standard free energies of adsorption were lower than 40 kJ mol^{-1} , confirming the physisorption of (Tyr). Surface analysis using EDX/SEM confirmed the results obtained from chemical and electrochemical measurements that an adsorbed film of the inhibitor protects steel surface against corrosion. All the results obtained from the methods employed are in reasonable agreement.

References

- Theus GS, Daniel PL (1983) In: Proceedings of the eighth international Brown Boveri symposium, Baden, Switzerland, p 185
- NACE Publication (1982) Corrosion testing of chemical cleaning solvents, vol 21 Materials performance, 3M, p 48
- Rothwell AN (1992) J Corros Prev Contr 39:113
- Mann GMW (1976) High temperature high pressure electrochemistry in aqueous solutions. NACE-4, Houston, p 34
- Ghanem WA, Bayyoumi FM, Ateya BG (1996) Corros Sci 38:1171
- Majnouni MD, Jaffer AE (2003) In: Chemical cleaning a boiler—an overview, International water conference, paper no IWC-03-34, Pittsburgh
- Port RD, Herro HM (1991) The Nalco guide to boiler failure analysis. McGraw-Hill, New York
- Arwood KI, Hale GL (1971) In: A method for determining need for chemical cleaning of high pressure boilers, American power conference, Chicago, vol 33, p 710
- Hargrave RE (1994) Mat Perform 33:51
- Natarajan S, Babu SPK (2006) Mater Sci Eng A432:47
- Natarajan S, Sivan V (2003) Corros Prev Cont 50:7
- Sathiyarayanan S, Jeyaprabha C, Muralidharan S, Venkatachari G (2006) Appl Surf Sci 252:8107
- Awad HS, Abdel Gawad S (2005) Anti-Corros Meth Mater 52:328
- Thomas JGN (1980) In: Proc 5th European symposium on corrosion inhibitors, Ann Univ Ferrara, NS, Sez V, p 453
- Behpour M, Ghoreishi SM, Gandomi-Niasar A (2009) J Mater Sci 44:2444. doi:10.1007/s10853-009-3309-7
- Balaji S, Upadhyaya A (2009) J Mater Sci 44:2310. doi:10.1007/s10853-008-3020-4
- Sundararajan G, Phani PS, Jyothirmayi A (2009) J Mater Sci 44:2320. doi:10.1007/s10853-008-3200-2
- Rao VS, Singhal LK (2009) J Mater Sci 44:2327. doi:10.1007/s10853-008-2976-4
- Okayasu M, Sato K, Okada K et al (2009) J Mater Sci 44:306. doi:10.1007/s10853-008-3053-8
- Gabriele R (2002) Corros Rev 20:509
- Lebrini M, Traisnel M, Lagrenee M, Memari B, Bentiss F (2008) Corros Sci 50:473
- Oguzie EE, Li Y, Wang FH (2007) J Colloid Interf Sci 310:90
- Aksut AA, Onal NA (1995) Bull Electrochem 11:513
- Kalota DJ, De S (1994) Corrosion 50:138
- Madkour L, Ghoneim M (1997) Bull Electrochem 13:1
- Gomma GK (1998) Bull Electrochem 12:456
- Morad MS, Hermas AA, Abdel-Aal MS (2002) J Chem Technol Biotechnol 77:486
- Ashassi-Sorkhabi H, Ghasemi Z, Seifzadah D (2005) Appl Surf Sci 249:408
- Amin MA, Abd El Rehim SS, Abdel-Fatah HTM (2009) Corros Sci 51:882
- Abdel-Rehim SS, Khaled KF, Abdel-Shafi NS (2006) Electrochim Acta 51:3267
- Bosch RW, Hubrecht J, Bogaerts WF, Syrett BC (2001) Corrosion 57:60
- Bosch RW, Bogaerts WF (1996) Corrosion 52:204
- Kus E, Mansfeld F (2006) Corros Sci 48:965
- Han L, Song S (2008) Corros Sci 50:1551
- Abdallah M, Helal EA, Fouda AS (2006) Corros Sci 48:1639
- Zhao T, Mu G (1999) Corros Sci 41:1937
- Abd El-Rehim SS, Hassan HH, Amin MA (2001) Mater Chem Phys 70:64
- Abd El-Rehim SS, Hassan HH, Amin MA (2002) Mater Chem Phys 78:337
- Khaled KF, Amin MA (2009) Corros Sci 51:2098
- Moretti G, Quartarone G, Tassan A (1996) Electrochim Acta 41:1971
- Jeyaprabha C, Sathiyarayanan S, Venkatachari G (2005) Appl Surf Sci 246:108
- Flitt HJ, Schweinsberg DP (2005) Corros Sci 47:2125
- Flitt HJ, Schweinsberg DP (2005) Corros Sci 47:3034
- Abd El-Rehim SS, Hassan HH, Amin MA (2002) Appl Surf Sci 187:279
- Barcia OE, Mattos OR, Pebere N, Tribollet B (1993) J Electrochem Soc 140:2825
- Deslouis C, Tribollet B, Mengoli G, Musiani MM (1988) J Appl Electrochem 18:374
- Macdonald JR (1987) Impedance spectroscopy. Wiley, New York
- Boukamamp BA (1980) Solid State Ionics 20:31
- International Report CT (1989) 89/214/128, University of Twente, Eindhoven, The Netherlands
- Benedetti AV, Sumodjo PTA, Nobe K, Cabot PL, Proud WG (1995) Electrochim Acta 40:2657
- Lorenz WJ, Mansfeld F (1981) Corros Sci 21:647
- McCafferty E, Hackerman N (1972) J Electrochem Soc 119:146
- Amin MA (2006) J Appl Electrochem 36:215
- Damaskin BB, Petrii OA, Batrakov B (1971) Adsorption of organic compounds on electrodes. Plenum Press, New York
- Do D (1998) Adsorption analysis: equilibria and kinetics. Imperial College Press, London, p 10
- Khamis E, Mellucci I, Lantanision RM, El-Ashry ESH (1991) Corrosion 47:677
- Donahue FM, Nobe K (1965) J Electrochem Soc 112:886

58. Durnie W, Marco RD, Jefferson A, Kinsella B (1999) *J Electrochem Soc* 146:1751
59. Martinez S, Stern I (2002) *Appl Surf Sci* 199:83
60. Martinez S (2003) *Mater Chem Phys* 77:97
61. El-Sherbini EF (1999) *Mater Chem Phys* 60:286
62. Bastidas JM, De Dambornea J, Vazquez AJ (1997) *J Appl Electrochem* 27:345
63. Mansfeld F (1987) *Corrosion Mechanism*. Marcel Dekkar, New York, p 119
64. Antropov LI, Makushin EM, Panasenko VF (1981) *Metal corrosion inhibitors*. Kiev, Technika
65. Hassan HH, Abdelghani E, Amin MA (2007) *Electrochim Acta* 52:6359
66. Amin MA, Abd El-Rehim SS, El-Sherbini EEF, Bayoumi RS (2007) *Electrochim Acta* 52:3588